JAERI-M
5399

MEASUREMENT OF DIFFERENTIAL THERMAL NEUTRON SPECTRA IN GRAPHITE POISONED WITH INDIUM, CADMIUM AND SAMARIUM BY TIME OF FLIGHT METHOD

September 1973

Fujiyoshi AKINO, Yoshihiko KANEKO,
Sami, F. HANNA, Ryosuke KUROKAWA
and Kenji KITADATE

日本原子力研究所
Japan Atomic Energy Research Institute

この報告書は，日本原子力研究所が JAERI-M レポートとして，不定期に刊行している研究報告書です．入手，複製などのお問合わせは，日本原子力研究所技術情報部（茨城県那珂郡東海村）あて，お申しこしください．

JAERI-M reports, issued irregularly, describe the results of research works carried out in JAERI. Inquiries about the availability of reports and their reproduction should be addressed to Division of Technical Information, Japan Atomic Energy Research Institute, Tokai-mura, Naka-gun, Ibaraki-ken, Japan.

JAERI-M 5399

Measurement of Differential Thermal Neutron Spectra in Graphite Poisoned with Indium, Cadmium and Samarium by Time-of-Flight Method

Fujiyoshi AKINO , Yoshihiko KANEKO , Sami, F. HANNA*
Ryosuke KUROKAWA , Kenji KITADATE

Division of Reactor Engineering, Tokai, JAERI

(Received August 24, 1973)

Differential neutron spectra were measured in the parallelepiped graphite assemblies ($80 \times 80 \times 40$ cm^3) with densities of 0.74~0.72 consisting of a homogeneous mixture of the powders of graphite and neutron absorber such as indium oxide, cadmium salfate and samarium oxide, by the time-of-flight method using a JAERI 120-MeV electron linear accelerator. The results were compared with those calculated by 50 energy groups one-dimensional S_4 approximation with neutron scattering kernel ENDF/A, Young and Koppel's model. In normalization between theory and experiment at 2 eV, the calculated spectra are lower than the measured ones at 0.1 eV by about 30~50%, far beyond the discrepancies expected from defects of the scattering kernel used in the calculation. The cause for this is possibly inaccurate treatment of the neutron leakage in the slowing-down energy region. To obtain experimental data for the high-temperature graphite piles, the piles should thus be dense and large enough to describe the neutron leakage during slowing-down to the thermal energy region by the discrete S_n method.

---

* IAEA fellow Atomic Energy Establishment, Cairo, Egipt

JAERI－M 5399

飛行時間法によるインジウム，カドミウムおよびサマリウムを添加した黒鉛中の微分中性子スペクトルの測定

日本原子力研究所東海研究所原子炉工学部
秋濃藤義・金子義彦・S.F.Hanna*
黒川良右・北館憲二

（１９７３年８月２４日受理）

黒鉛粒に均質に酸化インジウム，硫化カドミウムおよび酸化サマリウムの微紛を混合し，平行六面体形（８０×８０×４０cm^3）の不銹鋼製タンクに満した体系中の微分中性子スペクトルを１２０MeVのＬＩＮＡＣを中性子源とした飛行時間法により測定した。この実験結果は，Young－Koppel のモデルを使ったＥＮＤＦ／Ａの中性子散乱断面積を入力とする５０群のS_4 近似による計算結果と比較されたが，この黒鉛の散乱模型の不確さから予期される範囲を超える大きな理論，実験間の不一致がみとめられた。この原因は主として減速エネルギー領域における中性子漏洩の取扱いの不備によるものと推論された。
このため今後予定している高温領域における実験に対しては体系を拡大すると共に密度を高めれば，精密な実験，理論の比較が可能になることが判明した。

＊ＩＡＥＡ 留学生

目　次　な　し

Chap. 1 Introduction

The basic properties of the neutron scattering kernel of graphite for use in reactor core calculations have been studied in the following two ways. The first is the direct measurements of the scattering cross section $\sigma(E \rightarrow E')$ by use of the neutron diffraction or the time of flight method. The second is the measurements of the neutron spectra in graphite bulks poisoned with neutron absorbers mainly by the time of flight method. They have been closely complementary each other. The first is the most fundamental may whilst it has failed to yield accurate results in some specified energy ranges, from the experimental difficulties, and then the frequency distribution can't be determined only with the first type experiment. Therefore one has to determine theoretically the frequency distribution from the view point of solid state physics. The validity of the kernel, which is obtained through such a procedure, for the description of reactor spectra has been checked by comparing the measured neutron spectra in the graphite bulks with their calculated ones by use of the kernel under interest.

The measurements of the neutron spectra in the poisoned bulks have ever been extensively made by the groups of GA in USA and Harwell in UK., using electron linear accelerators. Parks et al.,[1] measured neutron spectra in the cubes of $(50\ \text{cm})^3$, poisoned with thin borated stainless steel sheets up to 0.4 b/c atom at temperature from 300°K to 810°K. Their experimental results showed good agreements with the calculated ones based on Parks model. Gayther et al.,[2] also measured the neutron spectra in a bulk of $(57\ \text{cm})^3$, poisoned with stainless sheets containing Cadmium or Boron up to 1.18 b/c atom. Their results for the cube poisoned with Cadmium showed considerably large disagreements with the calculated ones, using the Egelstaffs frequency distribution.[3]

In JAERI the measurements of the neutron spectra poisoned with Boron and Samarium are planned at high temperature up to 1100°K with aim to establish the validity of the graphite kernel of ENDF/A, Young and Koppels model for use in the design of high temperature gas cooled reactors. The present report discribes the measurement of the neutron spectra in the parallelepiped graphite assemblies ($80 \times 80 \times 40\ \text{cm}^3$) at room temperature. This experiment was made as a pre-step of the main plan at the high temperature. The characteristic points of the present work are firstly that poisoning of the graphite by the absorbers are made as homogeneously as possible by mixing absorber powders into pure graphite powders, and

secondly that slab like geometry is adopted for making it possible to get well defined distribution of the source neutrons, which are slowing down to thermal neutrons. Valuable experience and information are obtained for the design of the experimental assemblies to be used in the main plan for high temperature regions by applying theoretical analysis on the present experimental results.

Chap. 2 Experimental apparatus

1. Experimental assemblies and neutron collimation

The plan view of the JAERI electron linear accelerator facility is shown in Fig. 1. The set up of the experimental assemblies were stainless steel parallelepiped tanks filled with graphite powders, which homogeneously contained the powders of the neutron absorbers such as indium oxide, cadmium sulfate and samarium oxide. The tanks were 40 cm thick and 80 cm high, and covered with 0.6 mm thick cadmium sheets to make their boundaries black to the thermal neutrons. The concentrations of the added absorbers were changed, as shown in Table 1, to simulate the heavy buildup of ^{239}Pu and ^{240}Pu in the cores of usual graphite moderated reactors, and then they were named as No. 1, No. 2 and No. 3. The poisoned graphite powders of the experimental assemblies were prepared by the following two steps; the first is to make up the mother dispersed powders with high concentrations by use of bow mixer and the second is to dilute the mother powder to the specified concentrations by use of a V type mixer. After the tanks were filled with the powders, prepared above, they were vibrated vertically to get higher gross densities. The homogenity of the local density was checked by measuring the weight of the powders, taken-out from the tank for every 10 cm height. The distributions of the absorber concentrations were also measured by sampling the powders of about 10 g from various parts of the assemblies. The results of the chemical analysis of the sampled powders showed a remarkable homogenity throughout the tank, as shown in Table 2. The grain sizes of the powders of the absorbers were let to be so much small as the selfshieldings effect is completely negligible (See, Table 5). The graphite powders should preserve the essential properties of crystalline graphite for the thermal neutron scattering. Then, the diffraction pattern of the X rays was taken for the graphite powder, used in the No. 3 assembly. It is seen from Photo. 2 that its diffraction pattern is the same with that of the standard graphite.

To extract the 0°-directed neutron beam in the direction along the target to the center of the assembly, a reentrant hole with 40 mm diameter and 20 cm depth was provided on a side of the experimental assembly, facing the neutron flight tube, as shown in Fig. 2. The depth of the reentrant hole was changed by inserting the two plugs (3.8 cm dia. 4.5 cm high) containing the poisoned graphite powders, their concentrations being the same with those in the assembly. A tantalum target was placed apart

from the another side of the experimental assembly by a 5 cm thick lead layer to inject fast neutrons to the spectrum sources with the spatial distribution as sinusoidal as possible in the direction perpendicular to the target-center of the experimental assembly axis. The fast neutrons were provided by bombarding the tantalum target (See Fig. A-1) with an accelerated electron beam of about 300 mA from the JAERI 100 MeV linear accelerator, with a pulse width of 2 μ sec and a repetition frequency of 25 pps. The neutron beams from the reentrant hole was so collimated that only the neutrons leaving the bottom of the reentrant hole would reach the bank of four BF_3 counters after their flight through the evacuated neutron flight tube. The layout of neutron collimation is shown in Fig. 2. The evacuated flight tube, which is 18 ~ 70 cm in diameter and about 39.9 m long, had two thin aluminum windows, 0.5 mm and 2.0 mm thick. The total length of the neutron flight path, including the flight tube was 41.4 m, and energy resolution was better than 7 % for the whole energy range.

2. Neutron detection and flight time analysis

The block diagram for time analysis of the neutron counts is shown in Fig. 4. The neutrons were detected at the end of the flight path by a vertical single layer bank of four BF_3 counters, all of 5.0 cm diameter (20th century 40EB70). The detector bank has a 20 cm × 20 cm "square" window, and it is shielded from room scattered neutrons by Cd sheets and layers of B_4C and $NaBO_3$. The detection of neutrons in the detector bank was recorded on a ND 2200 512 channel time analyzer, which was operated in a mode of multi-scaling. Gold pins (20 mm in length, and 1 mm dia.) were used for monitoring the neutron yields from the tantalum target. For this purpose the pins, which were sandwiched between the two paraffin blocks, were irradiated at the inside corner of the target shield. The energy-dependent neutron detection efficiency of the detector bank is very important for the accurate conversion of the time distribution of neutron counts into the neutron flux-energy spectra. This neutron counting efficiency can be obtained well by calculation by means of the formula.

$$S(E) = e^{-(\Sigma_T^{air} T_{air} + \Sigma_T^{Al} T_{Al})} \cdot \int_0^R e^{-(\sqrt{(R+\ell)^2 - r^2} - \sqrt{R^2 - r^2})} \cdot \Sigma_T^{Cu} \cdot (1 - e^{-2\sqrt{R^2 - r^2}\,\Sigma_a^{10B}})\, dr, \qquad (1)$$

where

Σ_T^{air}, Σ_T^{Al}, Σ_T^{Cu} : Macroscopic total cross sections of air, Al, and Cu respectively,

Σ_a^{10B} : Macroscopic absorption cross section of ^{10}B

T_{air}, T_{Al} : Thicknesses of air and Al layers, respectively.

R : Radius of BF_3 counter

ℓ : Thickness of Cu wall of BF_3 counter.

The results of calculation are shown in Fig. 5.

3. Energy resolution

The energy resolution of measurements obtained with the experimental apparatus described above is determined by three factors:

(1) Neutron mean emission time from the experimental assemblies

(2) Channel width of the time analyzer

(3) Pulse width of the neutron bursts

The first-mentioned factor-neutron mean emission time - $\tau(E, r)$ -defined by the time moment of the time-dependent neutron flux induced by the pulsed neutrons, are calculated with the one-dimensional diffusion code TUD:

$$\tau(E, r) = \frac{\int_0^\infty t\phi(E, r, t)dt}{\int_0^\infty \phi(E, r, t)dt} = \frac{\psi(E, r)}{\phi(E, r)} \qquad (2)$$

where $\phi(E, r)$ and $\psi(E, r)$ are the respective solutions of the equations

$$(D\nabla^2 + \Sigma_a + \Sigma_s)\phi(E, r) = \int_0^\infty \Sigma(E' \to E)\phi(E', r)dE' + S(E, r) \qquad (3)$$

$$(D\nabla^2 + \Sigma_a + \Sigma_s)\psi(E, r) = \int_0^\infty \Sigma(E' \to E)\psi(E', r)dE' + \frac{\phi(E, r)}{v} \qquad (4)$$

the symbols used here being as commonly adopted.

Equation (2) is an extension of the method introduced by Young et al.,[4] for space-independent problems. The results of calculation with Eq. (2) are given in Fig. 6 for the different experimental assemblies at their center position.

The pulse width of the neutron burst and the channel width of the time analyzer were 2 and 100 μsec, respectively. These two factors should be considered at the same time; the sum of the two values, i.e.

102 μsec, is accountable only in the higher energy region (for 1 eV neutrons, the value amounts to about 3 % of the total flight time of 2993 μsec).

Chap. 3 Experimental results

1. Neutron spectra

After subtraction of backgrounds measured with a B_4C plug inserted at the bottom of the reentrant hole, and correction for the counting losses, the time spectra $N(t)$ of neutron counts were transformed into energy spectra $\phi(E)$ of neutron flux by means of the formula

$$\phi(E) = \frac{N(t)}{S(E)} \cdot \frac{\triangle t}{\triangle E} \qquad (5)$$

where

$\triangle t$: Channel width of the time analyzer

$\triangle E$: Energy width corresponding to $\triangle t$.

The results thus obtained for spectra from the three assemblies are shown in from Fig. 7 to Fig. 12. The effect of the reentrant holes are estimated so small as to be surely neglected, because their diameter is 4 cm, which is considerably smaller than $\lambda_{tr} \approxeq 6$ cm, which is the neutron transport length in the experimental assemblies[5].

2. Scurce of thermal neutrons

The spatial distributions of neutron flux at the giant resonance level of Au (4.9 eV) were measured by the conventional activation method, using Cd covered Au wire of 1 mm diameter. The measurements were done along the target-assembly center axis as well as in the direction transversal to the axis. The measured results are shown in Figs. 13 and 14. It is seen from the figures that the spatial distribution in the transversal direction is well sinusoidal with a buckling of 0.002234 cm^{-2}, this justifies the simplification adopted in analyzing the experimental assemblies to assume an infinite slab by taking into account of the transverse neutron leakage in the very simple form described in Chap. 4.

Chap. 4 Theoretical analysis

Scheme of the calculation of thermal neutron spectra in the three different experimental assemblies, which are used in this experiment as sources of thermal neutrons, is shown in Fig. 15. One may describes the calculations stepwise as follows:

(1) Computation of the Po component of the scattering kernel of graphite and source neutron spectrum in each assembly.

(2) Calculation of 0° angular thermal neutron spectrum in each assembly at each bottom of the reentrant holes.

1. Computation of the scattering kernel of graphite

Using the computer code PIXSE[6], the Po component of the scattering kernel of the graphite is calculated from the scattering law $S(\alpha, \beta)$ listed in ENDF/A for the energy range from 0.0 to 4.9 eV. This energy range is devided into 50 groups as shown in Table 3, choosing the group width as fine as possible especially near the resonance energies of the poisons in each assembly. The matrix elements of the energy transfer kernel are obtained by use of the maxwellian or the $\frac{1}{E}$ type distribution one, as the weighting function $W(E/KT)$ for the respective energy ranges below and above the thermal cut off energy, taken as 0.125 eV. Basic equations used in the computation of the kernel $\sigma\, n(E \to E')$ are as follows,

$$\sigma\, n(E \to E') = \int_{-1}^{1} \mu^n \sigma(E \to E', \theta)\, d\mu \qquad (6)$$

where $\mu = \cos\theta$, n is the order of the angular moments, E and E' and the initial and final energies. θ is the angle of neutron scattering and $\sigma(E \to E', \theta)$ is the differential scattering cross section which may be written in general form as,

$$\sigma(E \to E', \theta) = \frac{\sigma_b}{2kT} \sqrt{\frac{E'}{E}}\, e^{-\frac{\beta}{2}}\, S(\alpha, \beta) \qquad (7)$$

where σ_b is the bound atom scattering cross section.

In the present calculation the $S(\alpha, \beta)$ function is obtained in form of a table from the ENDF/A[7] data using Young-Koppel[8] bound model through the computer code GASKET[9]. The values of the total cross section of graphite obtained by the above procedure coincide well with the measured ones of BNL-325[10], as shown in Fig. 16. The average cosine in the neutron

scattering is also shown in Fig. 17. The 50 groups absorption cross sections of the poisons and other structural material used in the calculation are compiled by using the code PI2[11]. Neutron reflections from the boundary shielding materials are taken into account by considering 6 regions as shown in Table 4. The source term $S_g(E)$ which is the number of neutrons scattered into g-th group from 1/E spectrum above the upper limit of the thermal energy, E_m, is also calculated by the PIXSE program according to the following equation.

$$S_g(E) = \int_{El}^{E2} dE \int_{Em}^{\infty} \frac{\sigma n(E' \to E)}{E'} dE'$$

The source term is calculated for each energy group and for 66 space meshs spreading over the 6 region of the experimental assembly.

2. Augular neutron spectrum calculation

The thermal neutron spectrum in each experimental assembly is calculated by using the WDSN-Mark 2[12] code solving the transport equation by the Sn approximation. In the present calculation we used S_4 approximation to describe the angular dependence of the thermal neutron spectrum in each case. We find that rapid covergence can be obtained by using, as initial guess, the spectrum which has been calculated using one dimensional diffusion calculation by the TUD[13] code. Neutron leakage from the system has also been taken into consideration by adding the leakage correction factor $D(E)B^2$ to the absorption cross sections, where $D(E)$ and B^2 are the diffusion coefficient and experimental assemblies the transverse buckling of the assembly respectively. The buckling is calculated by fitting the measured activations of gold foils, which are distributed spatially in the transverse direction, to a cosine curve using a least squares method.

The results of the neutron spectrum calculations for the three experimental assemblies are shown in from Fig. 7 to Fig. 12 for comparison with the experimental results.

Chap. 5 Discussion

The calculated 0° angular thermal neutron spectra in the three poisoned graphite assemblies are compared with the measured ones in from Fig. 7 to Fig. 12. In these figures the normalization between the calculated and measured spectra are done at 2 eV, which is just before the giant resonance of Indium. It is clear from the figures that there are considerably large discrepancy between experiment and calculation. The calculated spectra are lower than the experimental one at 0.1 eV by about 44, 37 and 30 % for the No. 1, 2 and 3 experimental assemblies repectively. In every assembly, the discrepancy is pronounced with use of the deepest reentrant holes, i.e. (depth 20 cm). It is also to be noted here that the descripancy starts already in the slowing down energy regions of a few electron volts, where the chemical binding effect of graphite is week and the absorption of neutrons is also very small except that by Indium. Similar tendencies to the present works were reported by the American group of GA[14]. They measured the 90° angular neutron spectra in a fairly small powdered graphite bulk ($17\frac{1}{4}" \times 22\frac{9}{16}" \times 23\frac{1}{8}"$) poisoned with Samarium (0.4 b/c atom) and they compared the results with calculation based on the parks model[1] as shown in Fig. 18. In the figure, the calculated spectrum is lower than the experimental one by about 30 % at 0.1 eV. The group of Harwell[2] has also pointed out as shown in Fig. 19 that the calculated 90° angular spectrum in a cube ($57 \times 57 \times 57$ cm^3) poisoned with use of cadmium containing steel plates (1.18 b/c atom), which is obtained using the frequency spectrum of Egelstaff[3], is about 20 % lower than the measured spectrum at the same energy value. One should ask what is the main cause for the descrepancies discribed above. The following three points should discussed as the probable cause for this discrepancy.

(1) The self-shielding effect of the resonance neutron absorbers. The absorption cross sections of Indium, Cadmium and Samarium show very strong resonances, but their grain sizes in chemical form of indium oxide cadmium sulfate, or smarium oxide, which are used to make up the experimental assemblies are let to be so much small as the self-shielding effect is completely negligible (see Table 5). The photographs by electron microscope confirmed that the grain sizes of neutron absorbers are less than those values listed in the table (see Photo 3, 4 and 5).

(2) Defect in the kernel of graphite. In order to check the influence of the chemical binding effect between carbon atoms on the neutron spectrum, we made calculation for the experimental assembly No. 3 by use of the Free gas model. However, as shown in Fig. 20, the results are 60 % higher than those with the $S(\alpha, \beta)$ of ENDF/A at 0.1 eV, whilst they a e still lower than the measured spectrum. If the normalization were made at 0.3 eV, below this energy point the calculated spectrum with the bound atom model could show better agreement with the measured one than the ones with Free gas model did. This is due to the fact that, in this energy region, the neutron spectrum is more sensitive to the properties of the graphite kernel for the energy change of the scattering neutrons than the description of the neutron leakage, because the neutron leakage is much depressed by the neutron absorptions, which become rapidly large there. This excludes the possibility that the cause for the descrepancy is mainly due to some defect in the kernel of graphite.

(3) Inaccurate treatment of neutron leakage

Table 6 shows the deviation of the calculated neutron spectra from the measured one at both 0.1 and 0.3 eV. The latter energy point is just before the rapide rise of the neutron absorption cross section of Cadmium and Samarium. It is clear from the table that the calculated spectrum already becomes much lower than the measured ones at 0.3 eV, even if the lethargy interval from the normalizing point of 2 eV to 0.3 eV is about 1.7 times wider than the rest interval from 0.3 to 0.1 eV. This fact indicates that the treatment for the neutron leakage which is preferential especially above 0.3 eV, is inaccurate, or that considerably large number of neutrons are supplied from the paraffin blocks used for the target shielding through the lead layer adjacent to the stainless steel tank including the poisoned graphite powders.

To overcome the ambiguity explained above, one may suggest a comment for the future experiments at high temperature that the graphite assembly should be dense and large enough to let the influence of the neutron leakage as well as the spatial and energy distribution of the source neutron to the thermal neutrons on the neutron spectrum to be acceptably small, when use is made of the discrete Sn method.

Chap. 6 Conclusion

Measurements of the differential neutron spectra in the parallelepiped graphite assemblies ($80 \times 80 \times 40$ cm^3), which were homogeneously poisoned with the neutron absorbers, Indium, Cadmium and Samarium, were made by the time of flight method, using the 120 MeV electron linear accelerator. The results were compared with the calculated ones, which were obtained by appling the one dimensional discrete Sn code WDSN-Mark 2, with use of the scattering kernel of ENDF/A, Young and Koppels model. When the normalization between theory and experiment was done at 2 eV, the calculated spectra were lower than the measured ones in the thermal neutron energy range by about 30 to 50 % which was far outside of the range expected from the probable defect of the scattering kernel. The main cause for the discrepancies is estimated to be inaccurate treatments of the neutron leakage in the slowing down energy region. This suggests a comment for the future plan, which is aiming at obtaing experimental data in the high temperature graphite pile, that the pile should be dense as well as large enough to make it possible to describe the phenomena of neutron leakage by the discrete Sn method.

Appendix

The target, shown in Phots. A.1, was designed so as to produce fast neutrons as many as possible, when it was bombarded with high energy electrons (200 μA at maximum), accelerated by use of the JAERI 120 MeV linear accelerator. The multi-layers of thin tantalum metal plates (each about 1.5 mm in thickness) were adopted as the transfer material from electrons to neutrons because tantalum metal has high melting point as well as extinguished compatibility with water. The shape of the target was made spherical with a reentrant hole with depth of about two times radiation length of tantalum, with aim at the isotropic production of neutrons. The cut view of the target is shown in Fig. A-1. The space dependence of the heat generation in the tantalum layers, which is very important from the view point of heat removal problem (24 K watt at maximum), was estimated by calculation, as shown in Fig. A-2, taking into consideration of both ionization energy loss of electrons and electron pair creations of the bremsstrahlung X rays. Cooling water was circulated at a rate of 12 liter per minute in a closed system, which was connected with the outer water loop, through a heat exchanger. A thermocouple monitred the outlet temperature of the cooling water.

Acknowledgement

The authors express their thanks to Dr. H. Takekoshi and the members of the operating staff of the electron linear accelerator for the collaboration with the operation of the accelerator. Dr. Y. Gotoh (Thermal Reactor Physics Lab.) read and critisized this manuscript. Their indebtedness extends also to Mr. Thuchihashi (Thermal Reactor Phisics Lab.) who gave many valuable advice for the neutron spectrum calculations, to Mr. A. Nagai (Chemical Analysis Center) who made precise chemical analysis for the poisoned graphite powders, and to Mr. T. Watanabe (Section of Mechanical disign) who performed the mechanical design of the tantalum target.

References

1. Parks, D. E. et al : Nucl. Sci. Eng. 13, 306 324 (1962)
2. Gayther, D. B. and Goode, P. D. : AERE-R4794 (1964)
3. Egelstaff, P. A. : IAEA Symposium on Inelastic Scattering of Neutrons in Solids and Liquids, Chalk River, Sm-30/20 (1962)
4. Young, J. C. et al : Nucl. Sci. Eng. 18, 376 ~ 399 (1964)
5. Akino, F. and Kaneko, Y. : J. Nucl. Sci. Technol. 10(1), 45 ~ 53 (1973)
6. Macdongall, J. D. : AEEW-M318 (1968)
7. Honek, H. C. : BNL-8381 (1965)
8. Young, J. A. and Koppel, J. U. : J. Chem. Phys. 42(1), 357 ~ 364(1965)
9. Koppel, J. U. et al : GA-7417 (Rev) (1967)
10. Hughes, D. J. et al : BNL-325 (1958)
11. Thuchihashi, K. : JAERI-1200 (1971)
12. Green, C. : AEEW-R498 (1967)
13. Thuchihashi, K. et al : JAERI-memo 3834 (1969)
14. Neill, J. M. et al : GA-6753 (1965)

Table 1 Absorber content in experimental assemblies

Neutron absorber / Assembly number	Cd	In	Sm
Number 1 (ρ=0.725)	0.3 w/o (0.82 barn/c)	0.3 w/o (0.063 barn/c)	0
Number 2 (ρ=0.725)	0.3 w/o (0.82 barn/c)	0	0
Number 3 (ρ=0.742)	0	0	0.3 w/o (1.40 barn/c)

: Gross density of the powders used to make up the experimental assemblies

(X) : Absorption cross section per a carbon atom at 2200 m/sec

Table 2 Results of chemical analysis for absorber content in experimental assemblies

Sample name	In (w/o)	Cd(w/o)	Sm(w/o)
1 - 1 - 2	0.309	0.289	
1 - 1 - 6	0.305	0.297	
1 - 2 - 2	0.300	0.294	
1 - 2 - 7	0.299	0.292	
1 - 3 - 2	0.299	0.294	
1 - 3 - 9	0.302	0.294	
2 - 1 - 2		0.298	
2 - 1 - 9		0.297	
2 - 2 - 1		0.305	
2 - 2 - 9		0.305	
2 - 3 - 1		0.301	
2 - 3 - 9		0.304	
3 - 1 - 1			0.293
3 - 1 -10			0.295
3 - 2 - 1			0.295
3 - 2 - 8			0.296
3 - 3 - 1			0.295
3 - 3 - 5			0.291

Sample name X-r-2 means that it was taken from at height Z of hole Y, digged in the experimental assembly X.

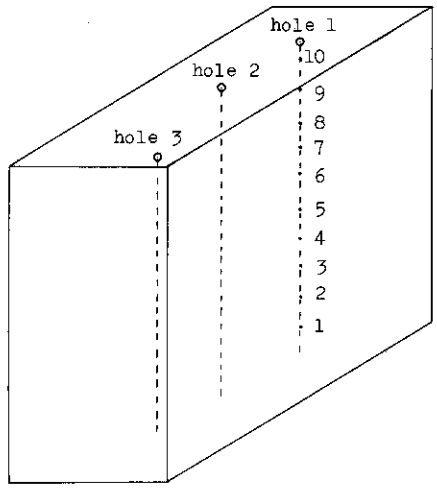

Experimental assembly

Table 3 Energy group division in neutron spectrum calculations

Groups	Upper energy (eV)	Lower energy (eV)	Groups	Upper energy (eV)	Lower energy (eV)
1	4.9	4.25	26	0.200	0.185
2	4.25	3.75	27	0.185	0.175
3	3.75	3.25	28	0.175	0.165
4	3.25	2.95	29	0.165	0.155
5	2.95	2.25	30	0.155	0.145
6	2.25	1.90	31	0.145	0.135
7	1.90	1.70	32	0.135	0.125
8	1.70	1.50	33	0.125	0.115
9	1.50	1.48	34	0.115	0.105
10	1.48	1.42	35	0.105	0.095
11	1.42	1.38	36	0.095	0.090
12	1.38	1.22	37	0.090	0.085
13	1.22	1.08	38	0.085	0.075
14	1.08	0.92	39	0.075	0.065
15	0.92	0.88	40	0.065	0.060
16	0.88	0.72	41	0.060	0.050
17	0.72	0.68	42	0.050	0.040
18	0.68	0.525	43	0.040	0.030
19	0.525	0.425	44	0.030	0.020
20	0.425	0.375	45	0.020	0.015
21	0.375	0.325	46	0.015	0.010
22	0.325	0.280	47	0.010	0.009
23	0.280	0.260	48	0.009	0.008
24	0.260	0.220	49	0.008	0.007
25	0.220	0.200	50	0.007	0.0

Table 4 Geometry of the experimental assembly adopted in the neutron spectrum calculation

Region number	Thickness (cm)	Space mesh point	Material	Atomic number (x 10^{24} atoms/cm^3)
1	5.	4	Pb	0.0330
2	0.06	6	Cd	0.0464
3	0.2	2	Fe	0.0848
4	40.	42	Poisoned graphite powder	C Cd In Sm H_2O No. 1 : 0.03601, 0.1166×10^{-4}, 0.1141×10^{-4}, 0.0, 0.1189×10^{-4} No. 2 : 0.03622, 0.1165×10^{-4}, 0.0, 0.0, 0.8492×10^{-5} No. 3 : 0.03708, 0.0, 0.0, 0.8914×10^{-5}, 0.1465×10^{-4}
5	0.4	2	Fe	0.0848
6	2.0	10	B4C	0.0109

Region number	1	2	3	4	5	6
	Pb	Cd	Fe	Poisoned graphite powder	Fe	B_4C

Table 5 Physical and chemical characteristics of the powder used to make up the experimental assemblies

Item / Absorber et al	Chemical state	Purity	Grain size
Graphite	Graphite powder	Ach < 0.087%	3 ~ 30 μ
Cd	CdS	99.9%	0.05 ~ 0.4 μ (Photo. 3)
In	In_2O_3	99.9%	< 2 μ (Photo. 4)
Sm	Sm_2O_3	99.9%	< 1 μ (Photo. 5)

Table 6. Discrepancies between measured thermal neutron spectra and calculated ones

	$1 - \frac{\text{calculated flux}}{\text{measured flux}}$					
Assembly	No. 1		No. 2		No. 3	
Reetrant hole depth (cm) / Energy (eV)	20.	10.8	20.	10.8	20.	10.8
0.3	0.29	0.32	0.24	0.23	0.14	0.095
0.1	0.[illegible]	0.45	0.31	0.41	0.31	0.17
0.025	0.41	0.68	0.55	0.63	0.53	0.13

Note: Po kernel and source, S_4, 6 regions, Young-Koppel model

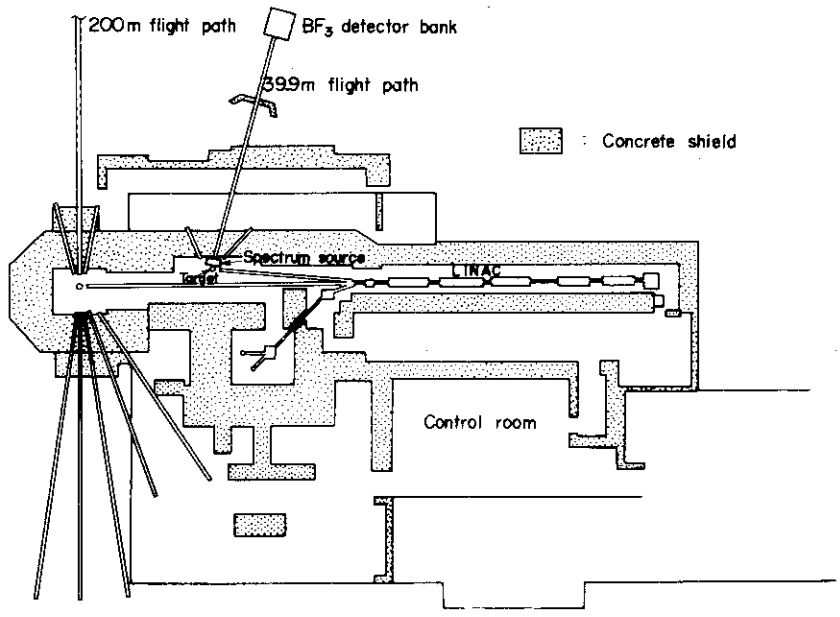

Fig. 1 JAERI 120 MeV LINAC facility

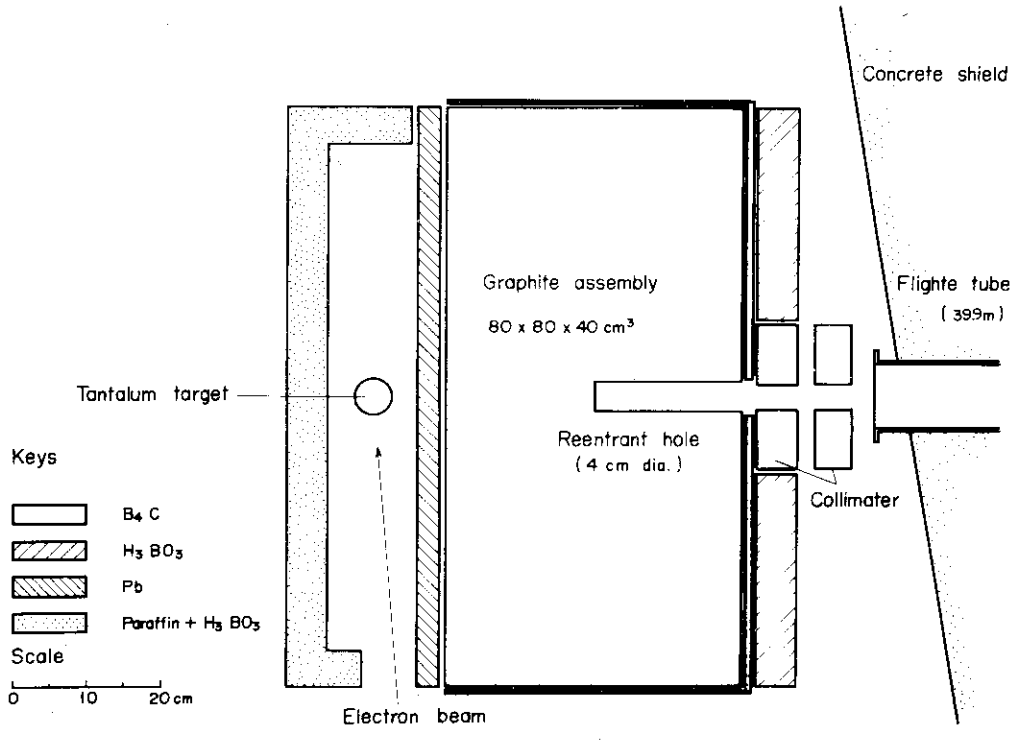

Fig. 2 Layout of experimental assembly

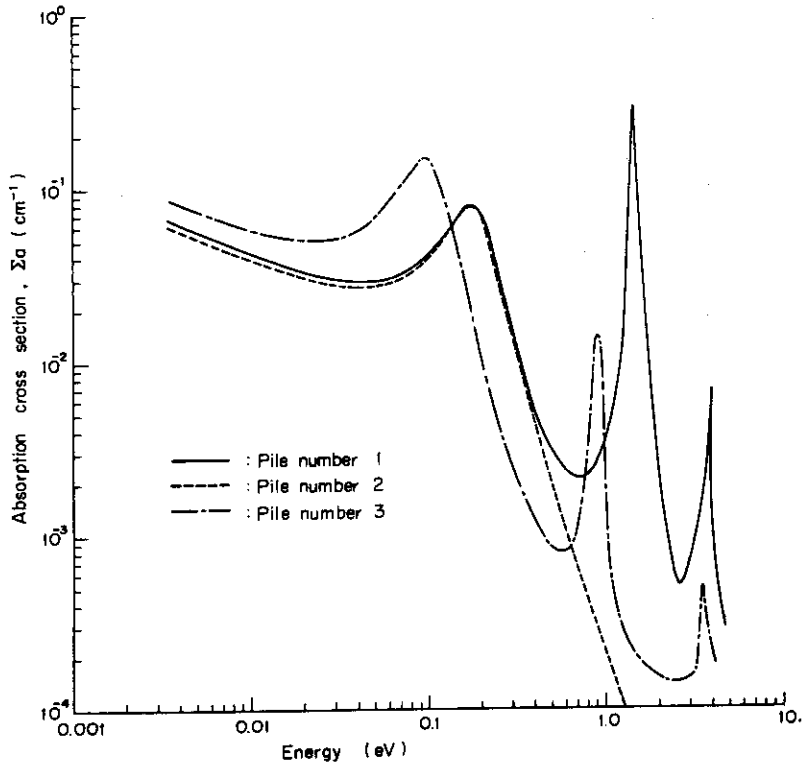

Fig. 3 Macroscopic absorption cross sections in experimental assemblies

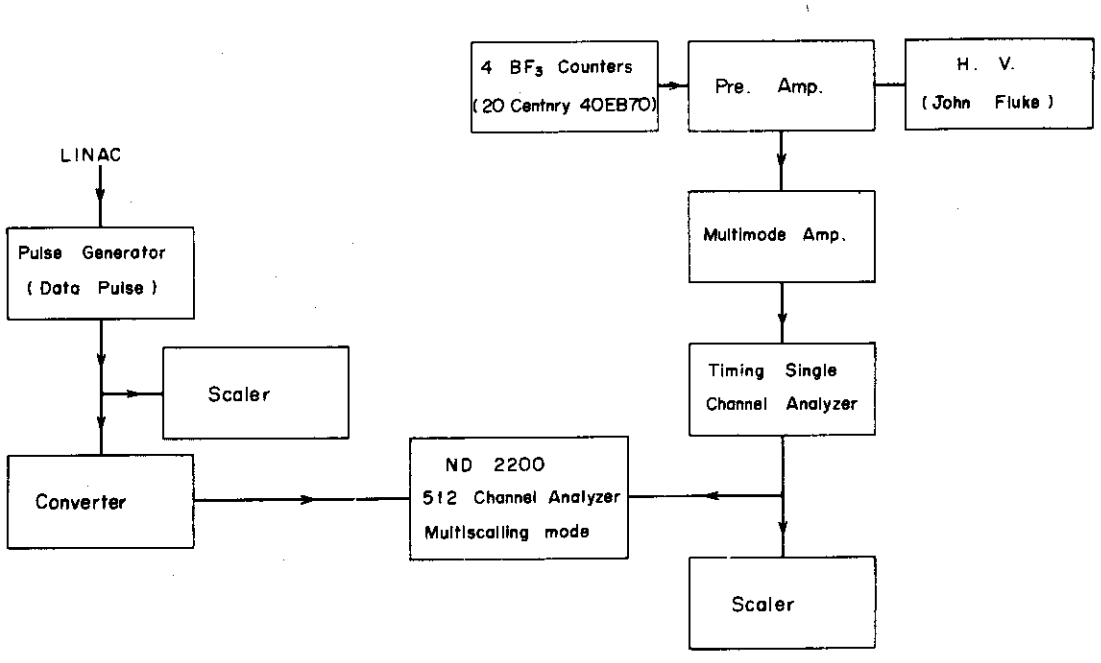

Fig. 4 Block diagram for time of flight measurement

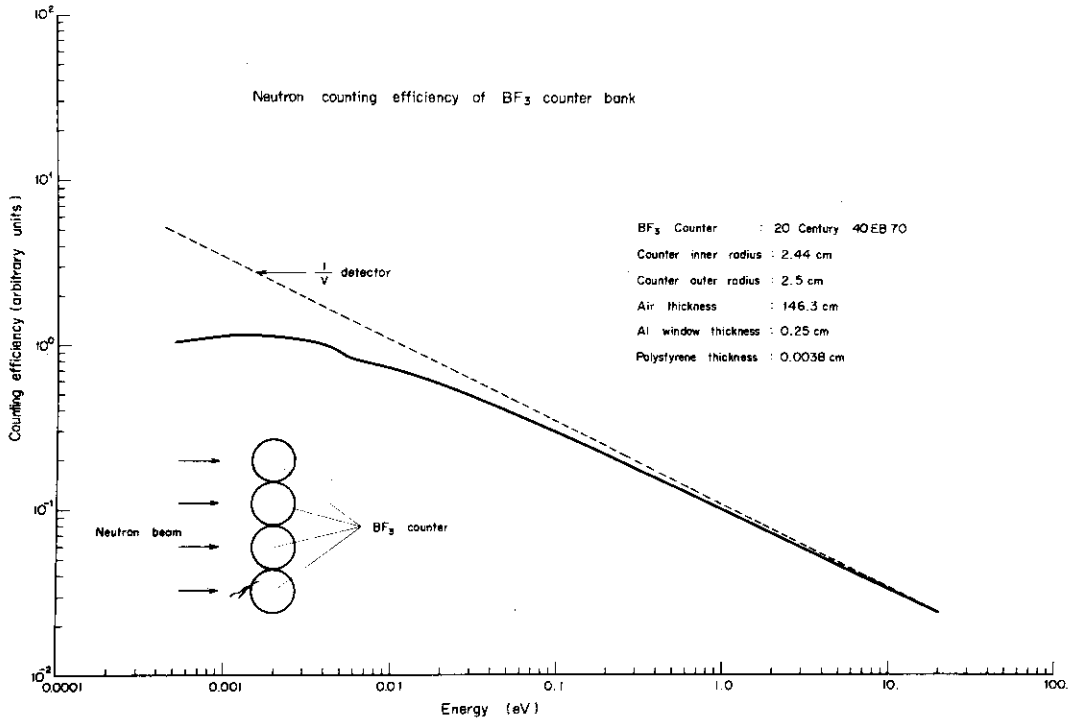

Fig. 5 Neutron counting efficiency of BF_3 counter bank

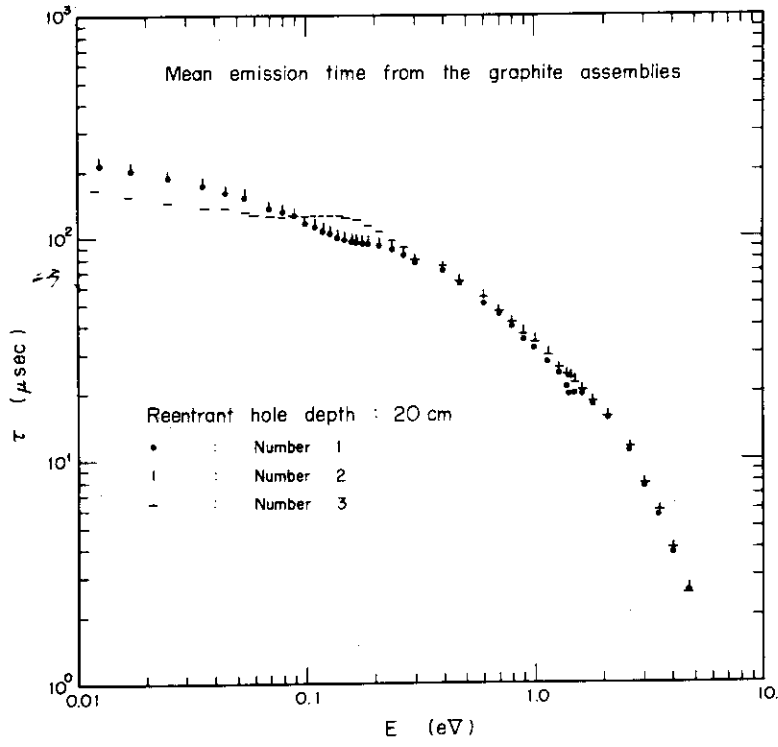

Fig. 6 Calculated mean emission times for experimental assemblies at their center

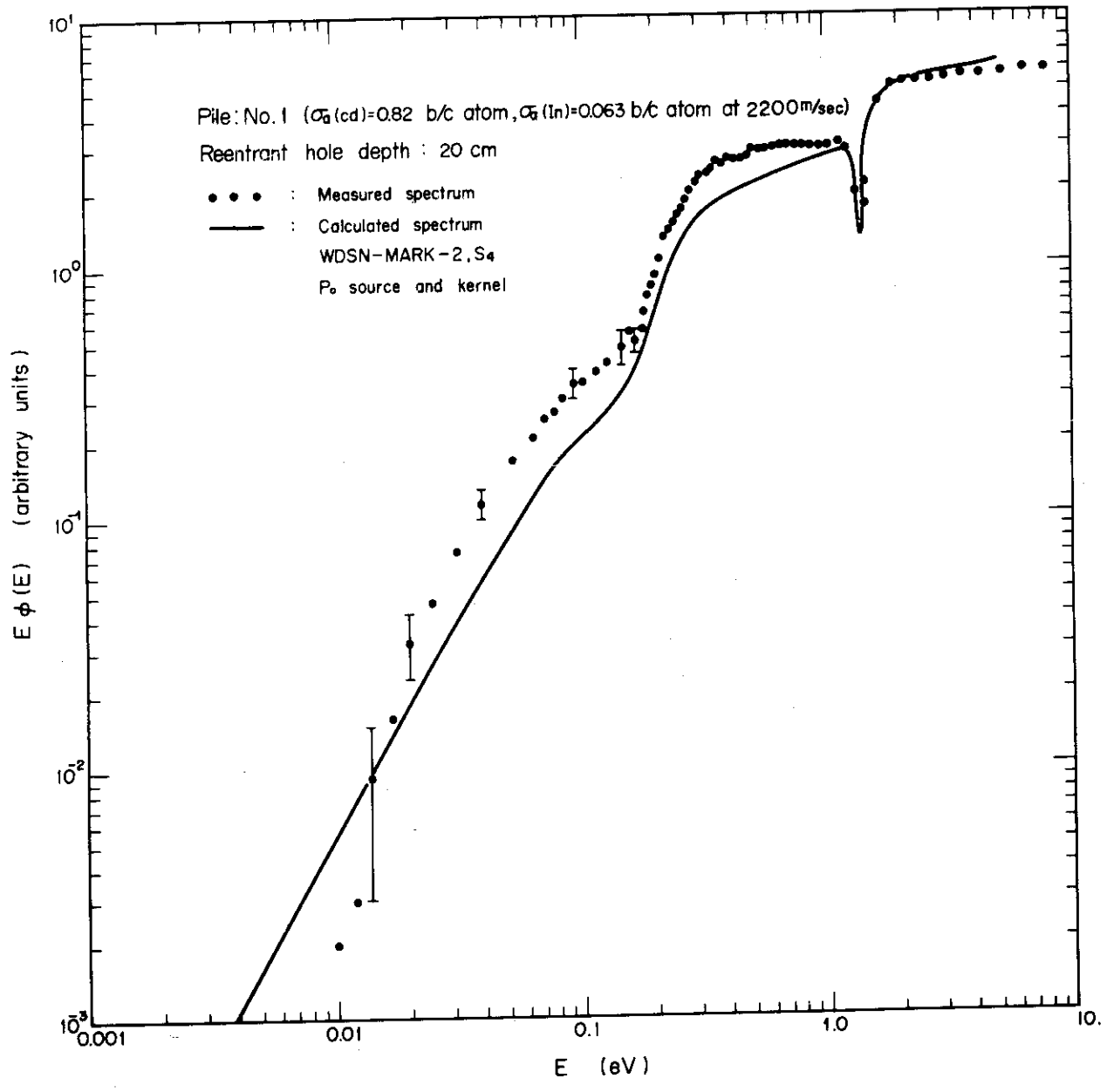

Fig. 7 Comparison of measured 0° angular thermal neutron spectrum with calculated one for the cadmium and indium poisoned graphite assembly No. 1 in case of the neutron beams being extracted from its center.

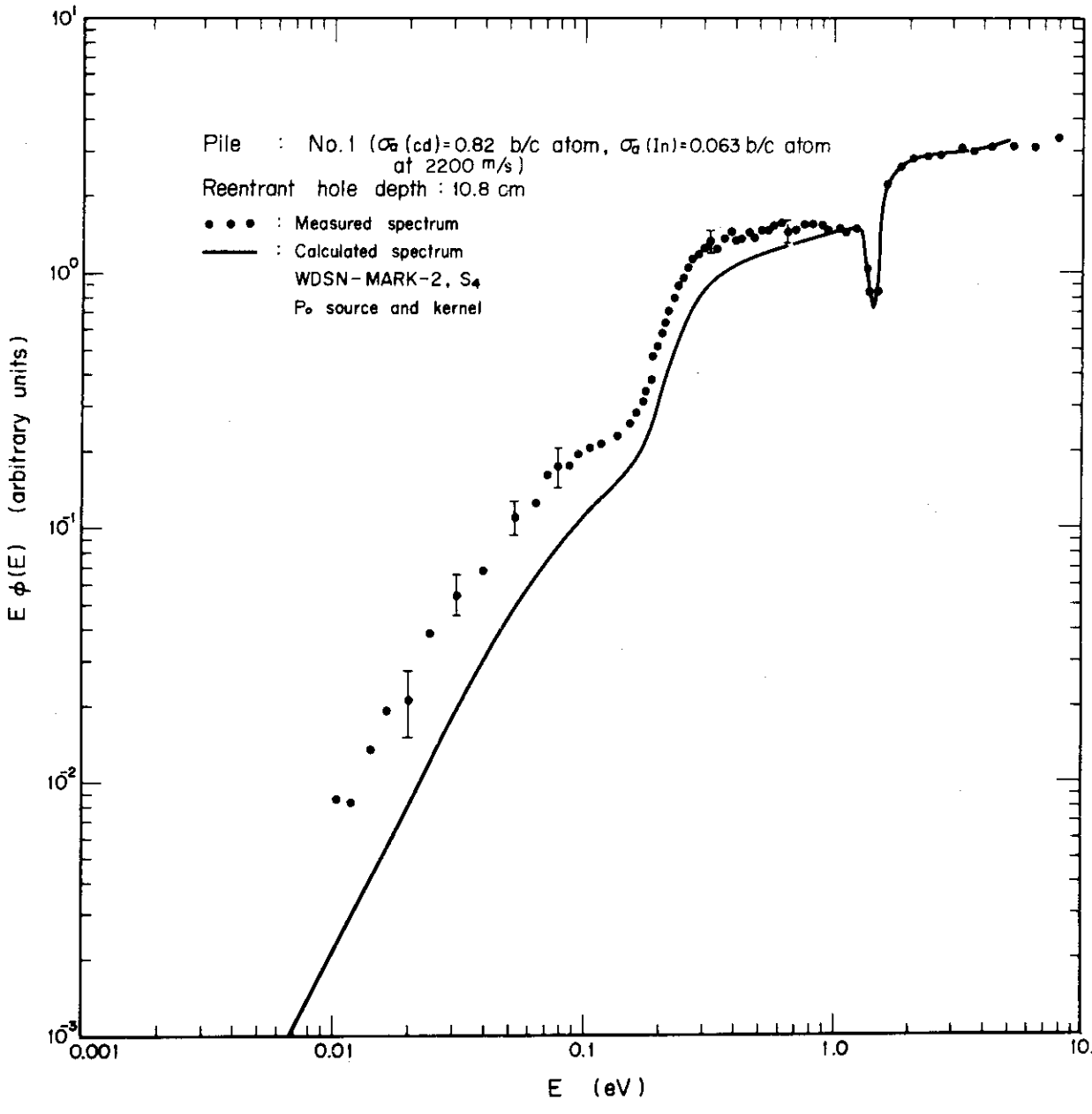

Fig. 8 Comparison of measured 0° angular thermal neutron spectrum with calculated one for the cadmium and indium poisoned graphite assembly No. 1 is case of the neutrons beams being extracted from the bottom of the 10.8 cm long reentrant hole.

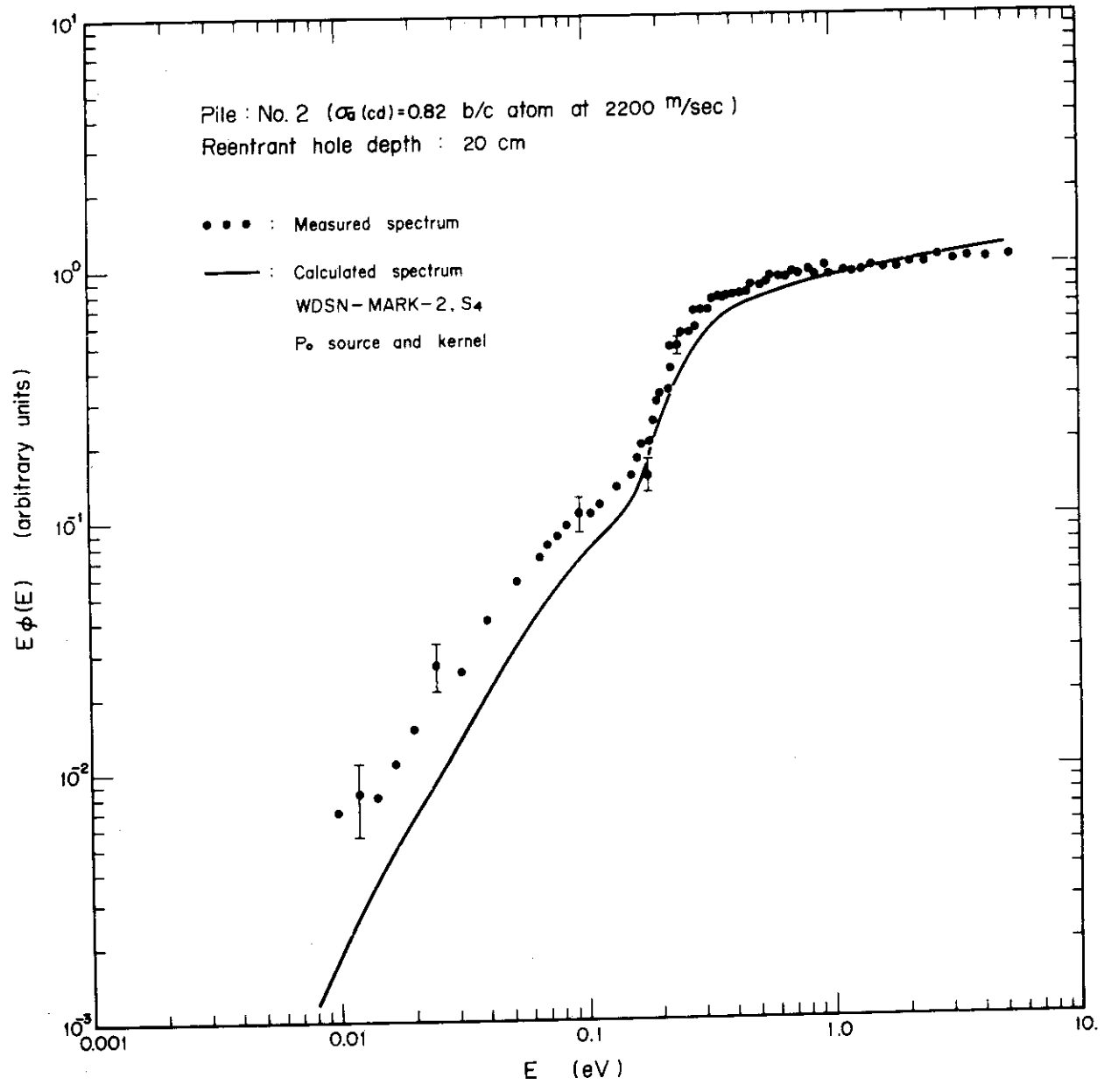

Fig. 9 Comparison of measured 0° angular thermal neutron spectrum with calculated one for the cadmium poisoned graphite assembly No. 2 in case of the neutron beams being extracted from its center.

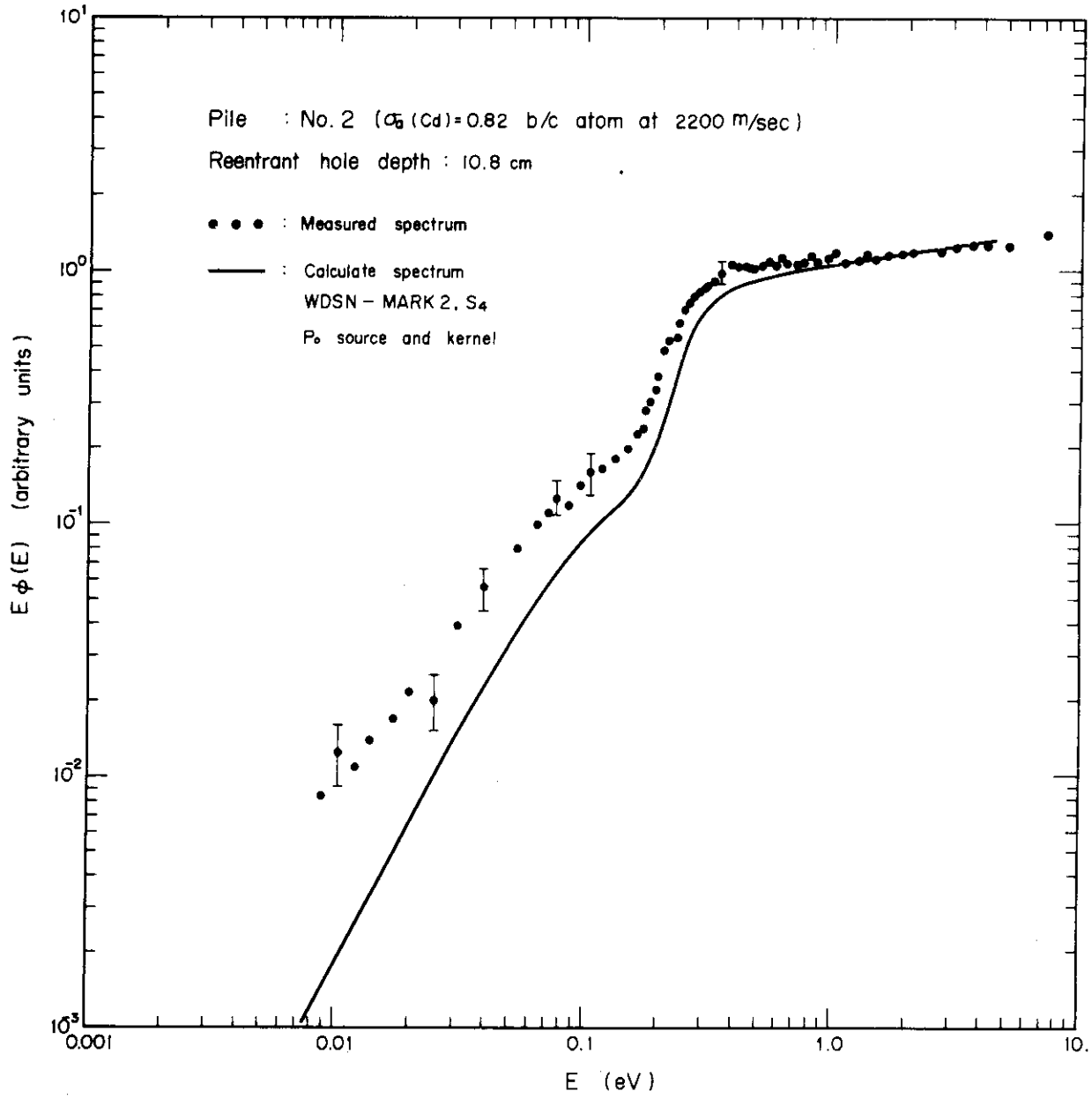

Fig. 10 Comparison of measured 0° angular thermal neutron spectrum with calculated one for the cadmium poisoned graphite assembly No. 2 in case of the neutron beams being extracted from the bottom of the 10.8 cm long reentrant hole.

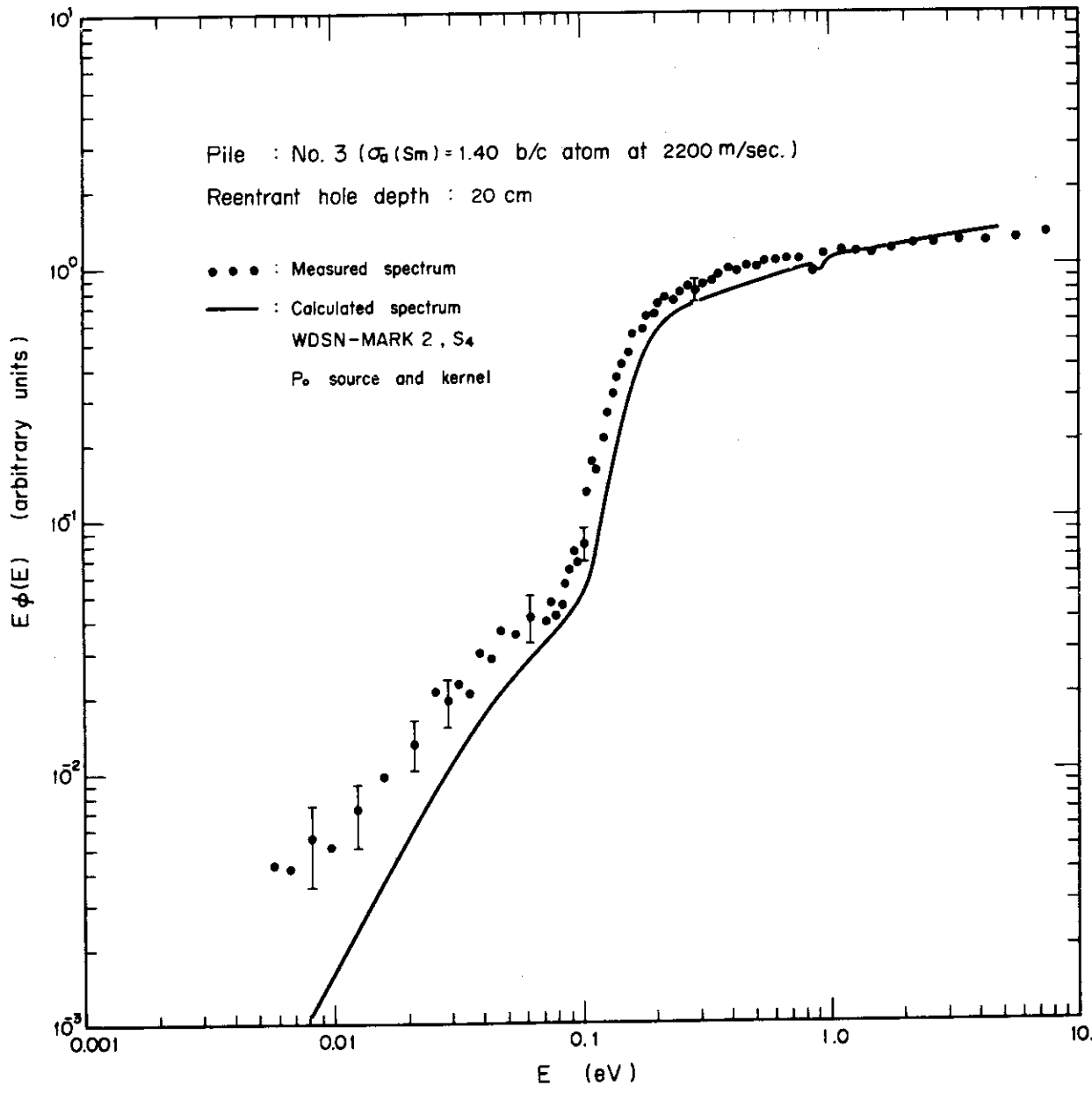

Fig. 11 Comparison of measured 0° angular thermal neutron spectrum with calculated one for the samarium poisoned graphite assembly No. 3 in case of the neutron beams being extracted from its center.

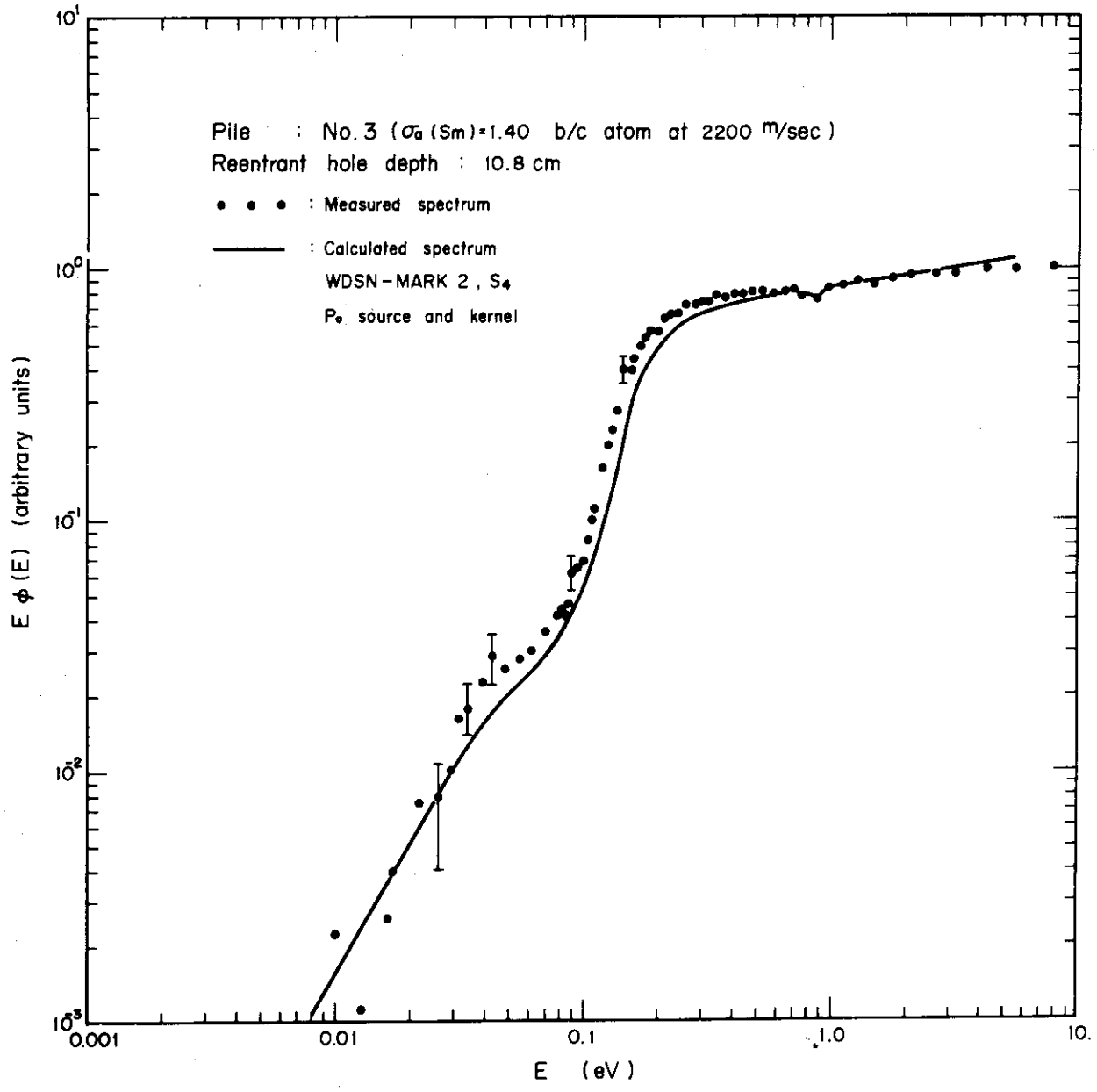

Fig. 12 Comparison of measured 0° angular thermal neutron spectrum with calculated one for the samarium poisoned graphite assembly No. 3 in case of the neutron beams being extracted from the bottom of the 10.8 cm long reentrant hole.

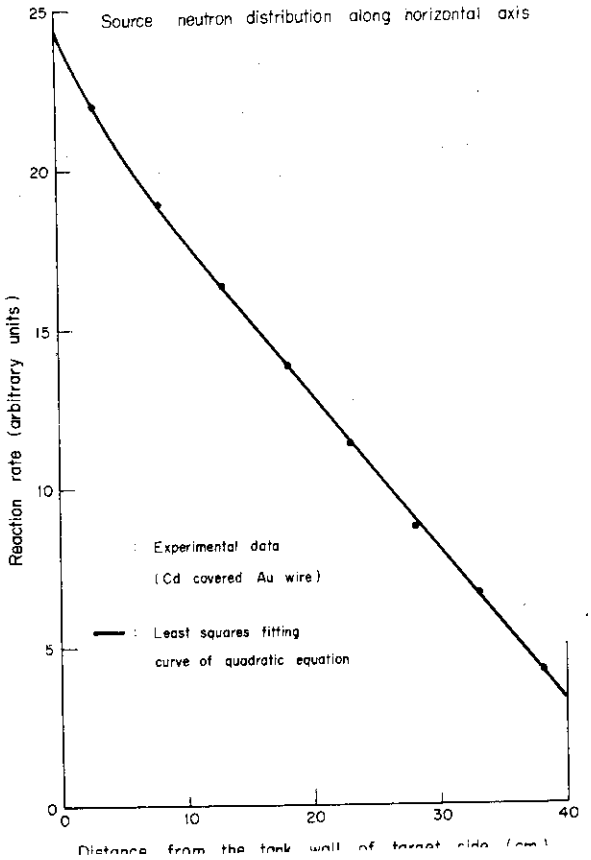

Fig. 13 Source neutron distribution along the horizontal axis of the experimental assembly No. 3.

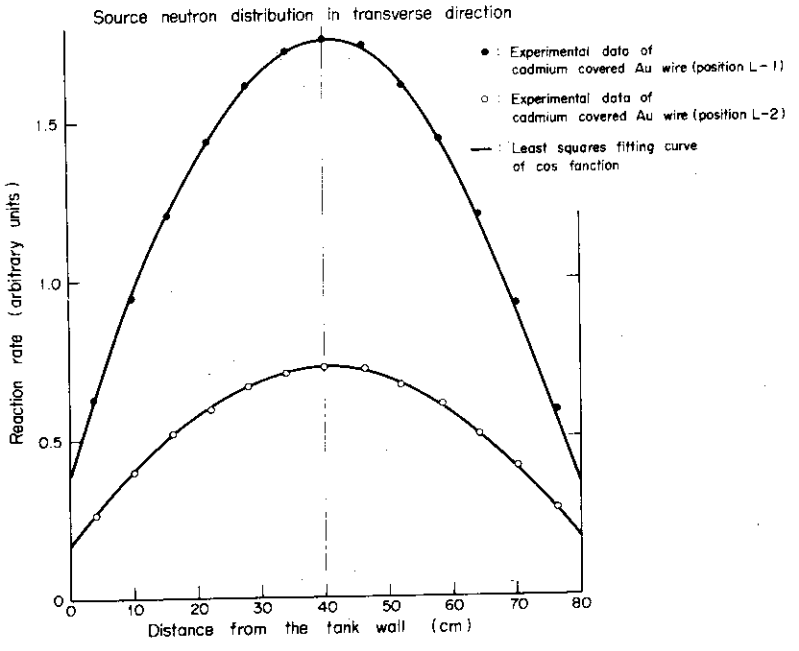

Fig. 14 Source neutron distribution in the transverse direction of the experimental assembly No. 3.

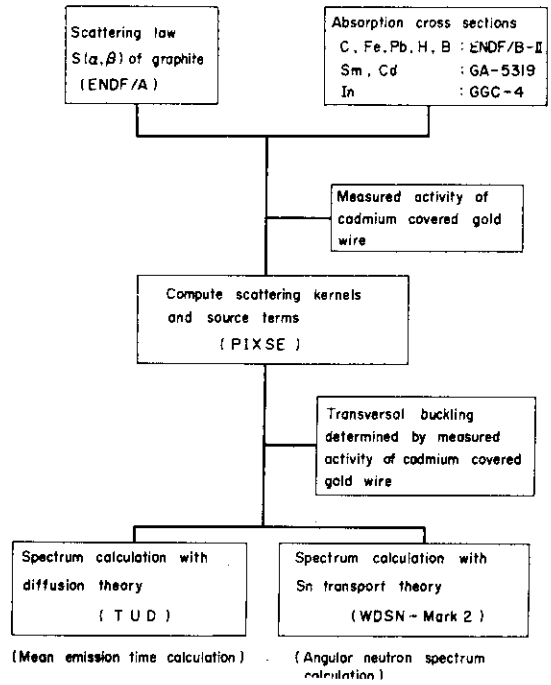

Fig. 15 Block diagram for calculation of thermal neutron spectra.

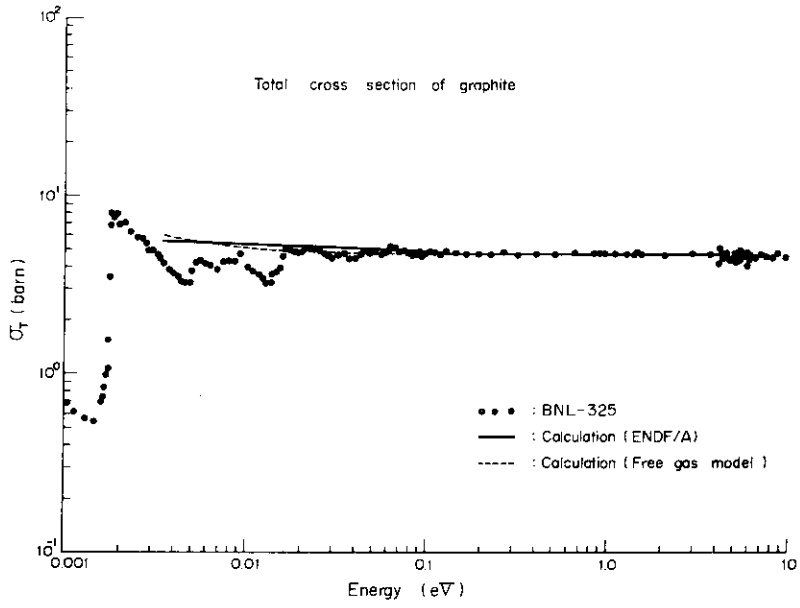

Fig. 16 Comparison of total cross section of graphite used in theoretical analysis with experimental data given in BNL-325.

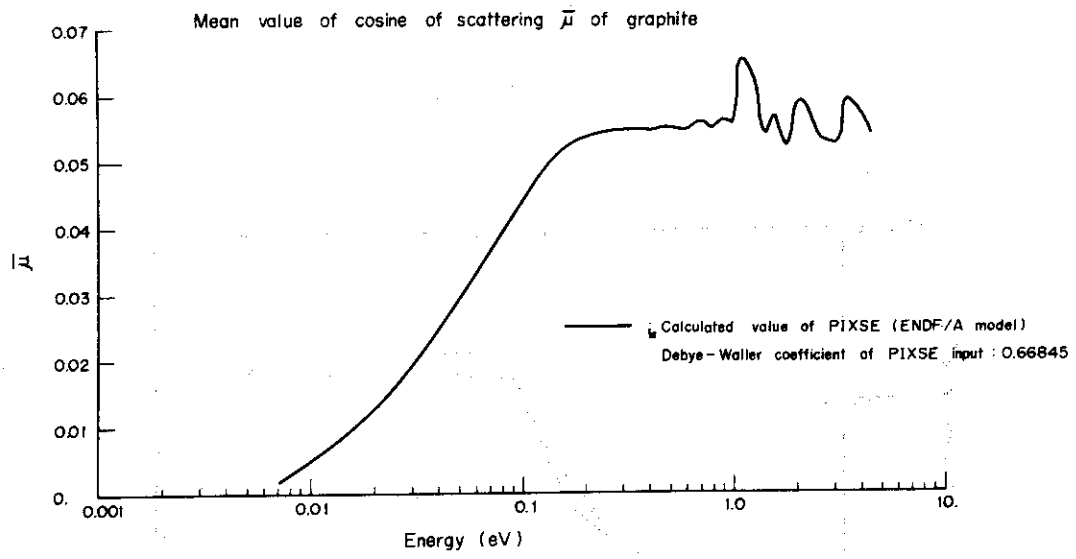

Fig. 17 Mean value of neutron scattering cosine by graphite.

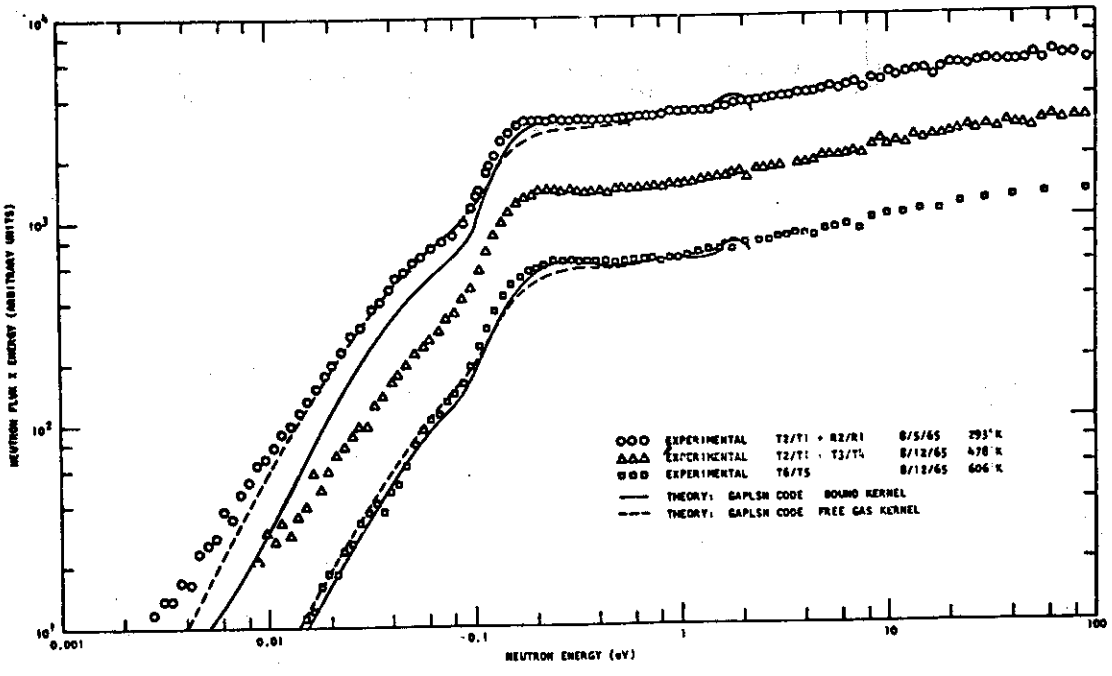

Fig. 18 Neutron spectra in samarium poisoned graphite at various temperatures reported by Neil, J. M. et al.

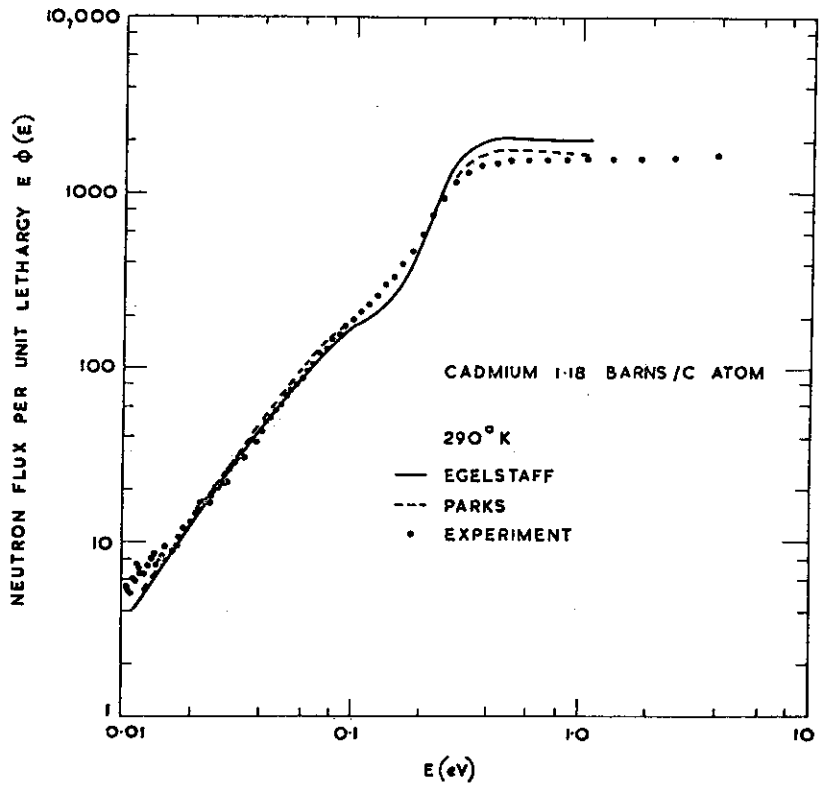

Fig. 19 Neutron spectra in cadmium poisoned graphite reported by Gaythor, D. B. et al.

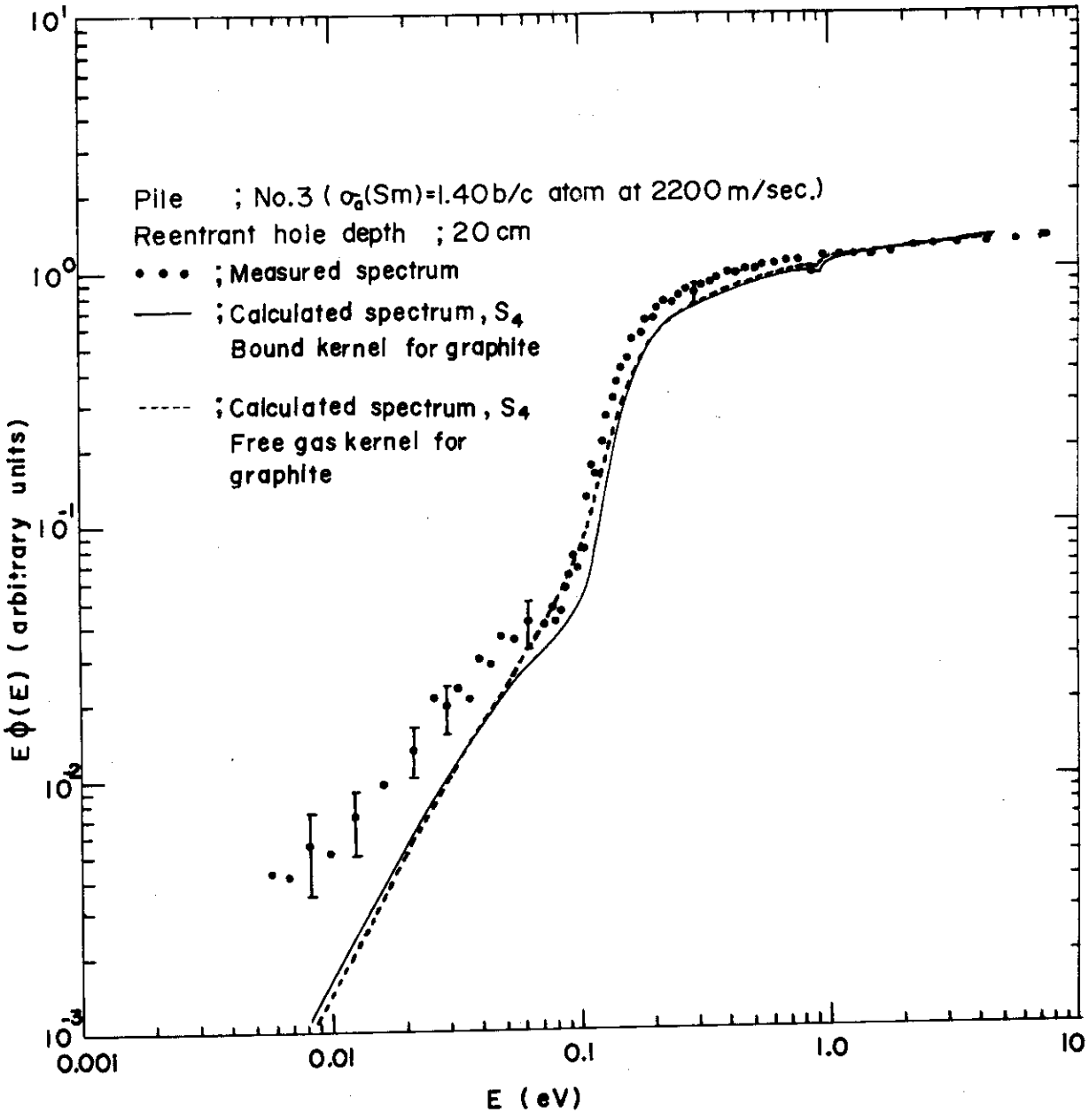

Fig. 20 Comparison of the measured 0° angular thermal neutron spectrum in the samarium poisoned graphite assembly (No. 3) with the calculated ones with the Young-Koppel or with the Free gas kernel.

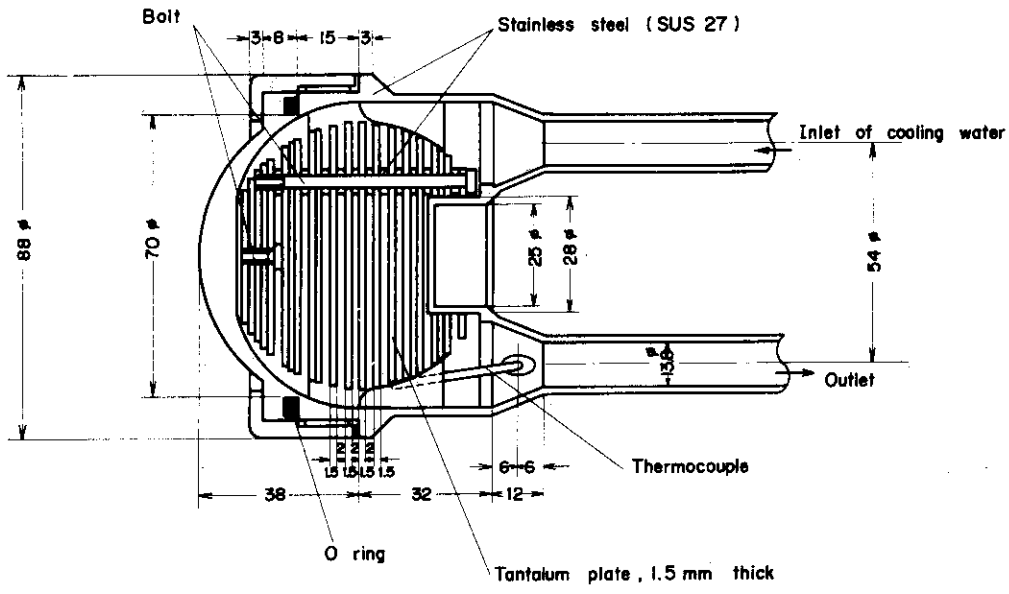

Cut view of target

Fig. A-1 Cut view of the target used in the experiment.

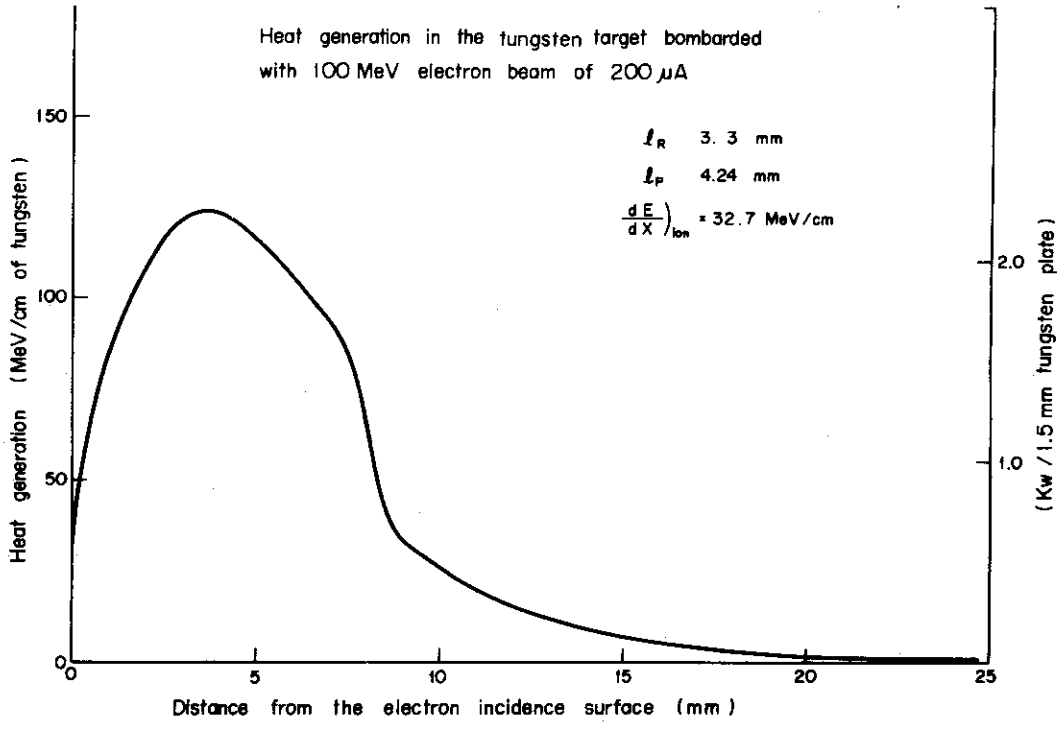

Fig. A-2 Heat generation in the tungsten target bombarded with 100 MeV electron beam of 200 μA.

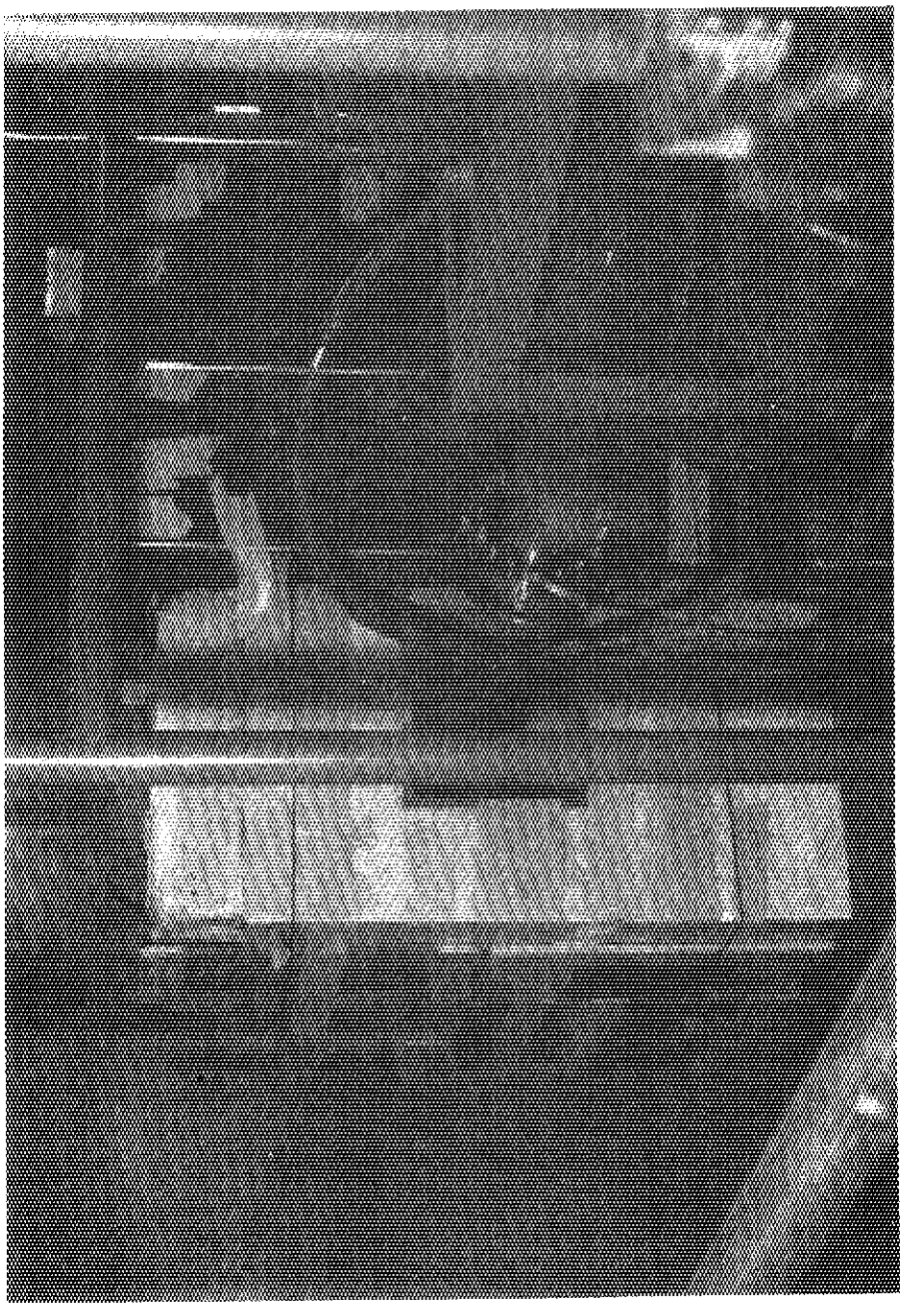

Photo. 1 Experimental assembly

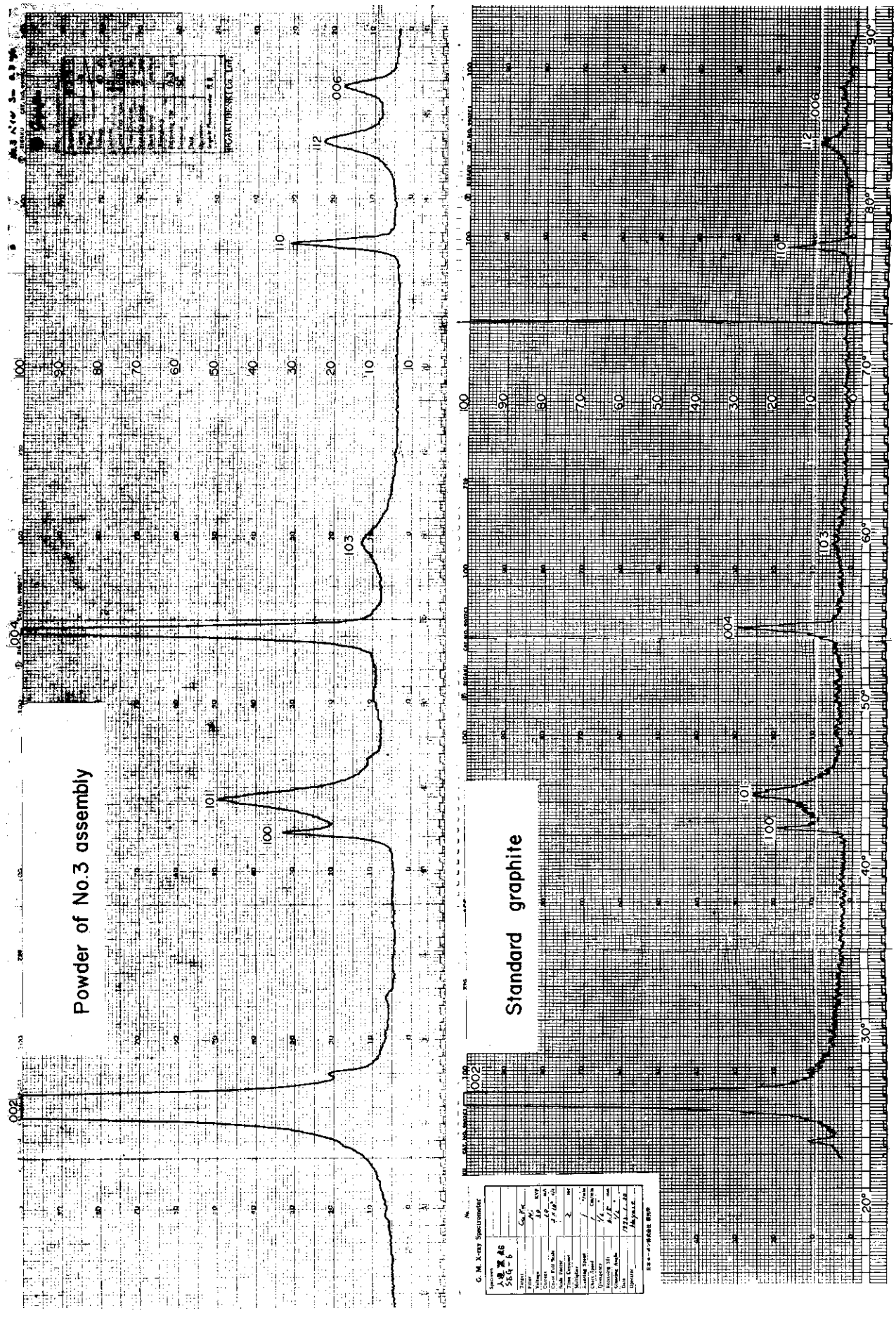

Photo. 2 Diffraction patterns of the X rays for the poisoned graphite powders of the No. 3 assembly and the standard graphite.

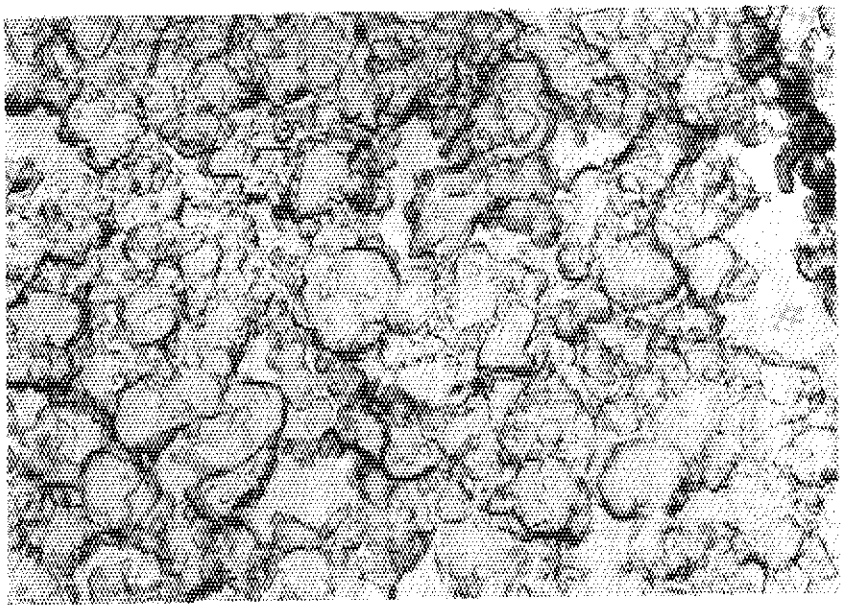

(cubic crystal)

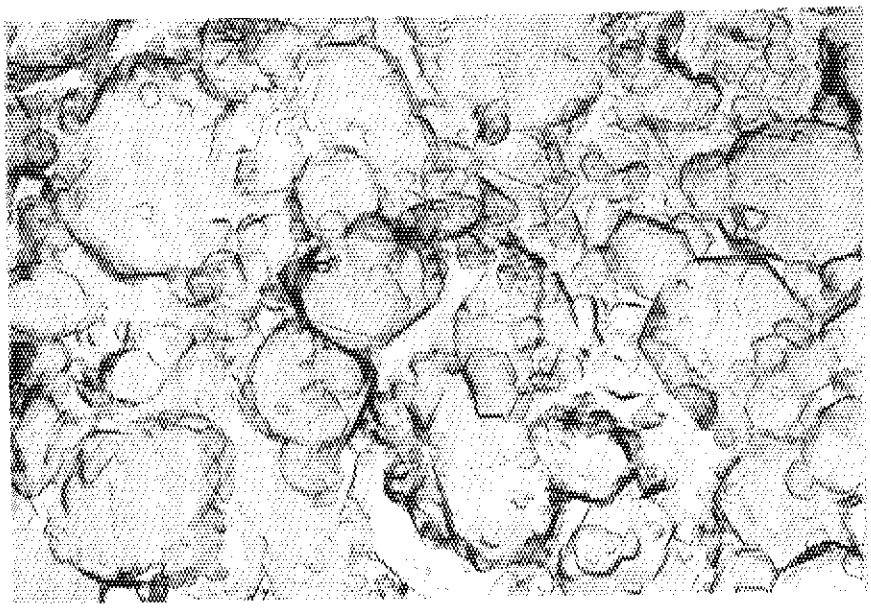

(hexagonal crystal)

Photo. 3 Electron microscopic photograph of CdS (replica method), (magnification: 15,000)

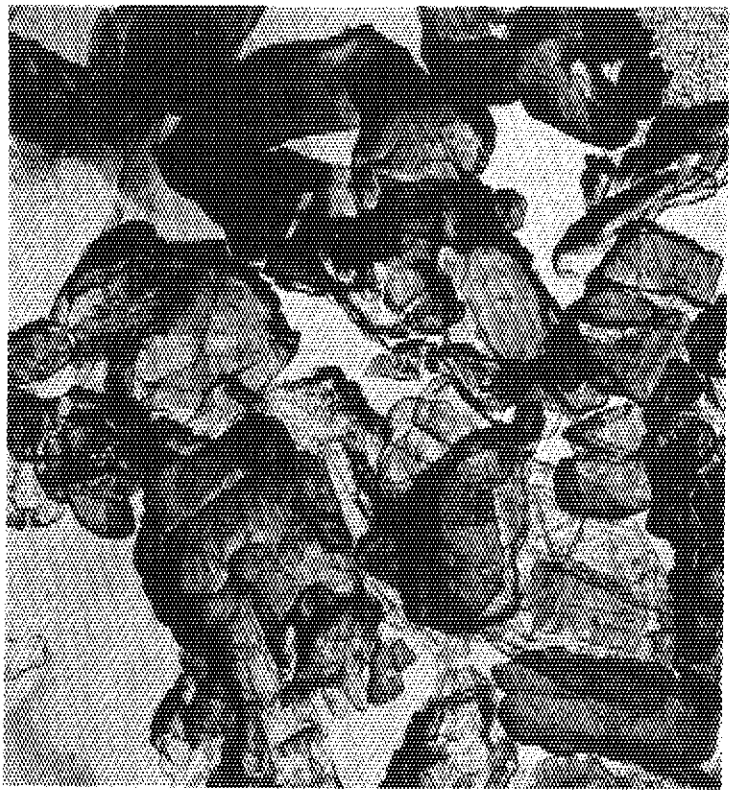

Photo. 4 Electron microscopic photograph of Sm_2O_3
(magnification: 10,000)

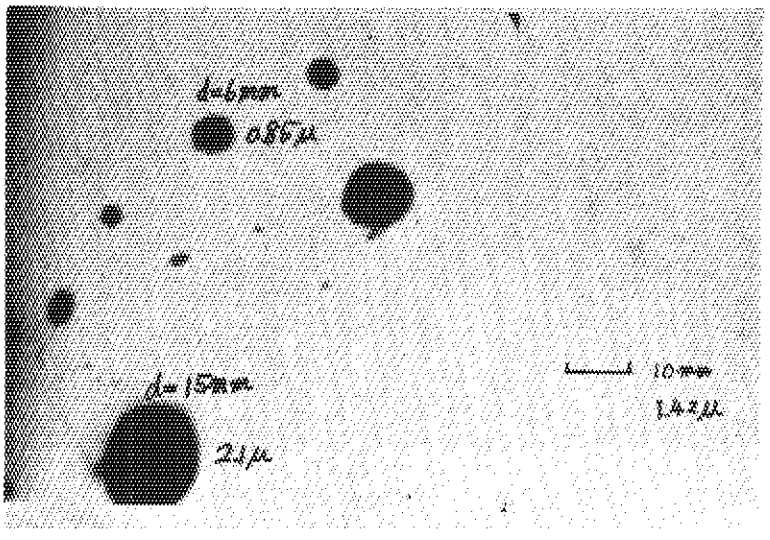

Photo. 5 Electron microscopic photograph of In_2O_3
(magnification: 7,000)

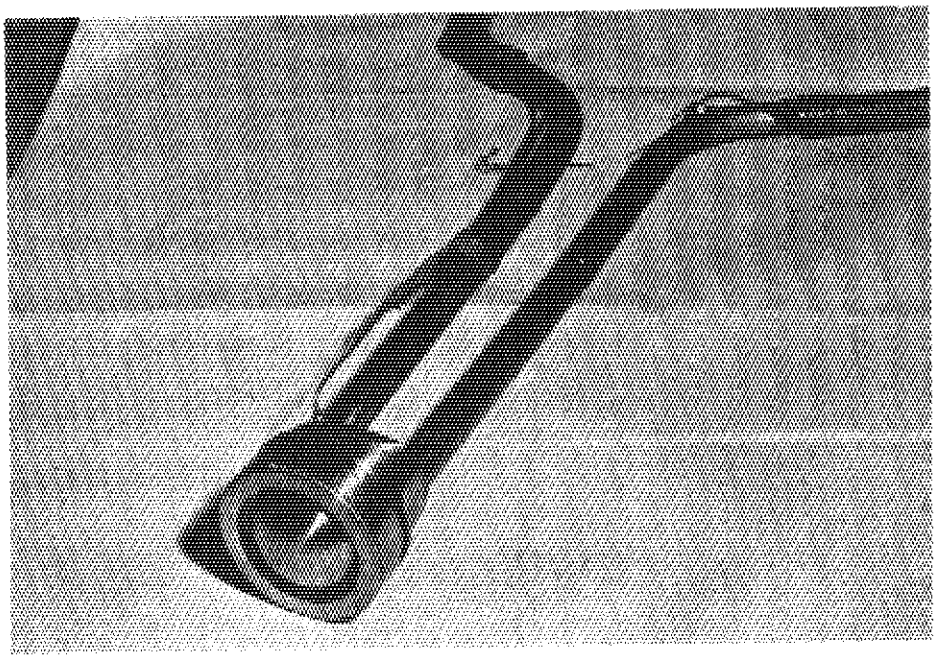

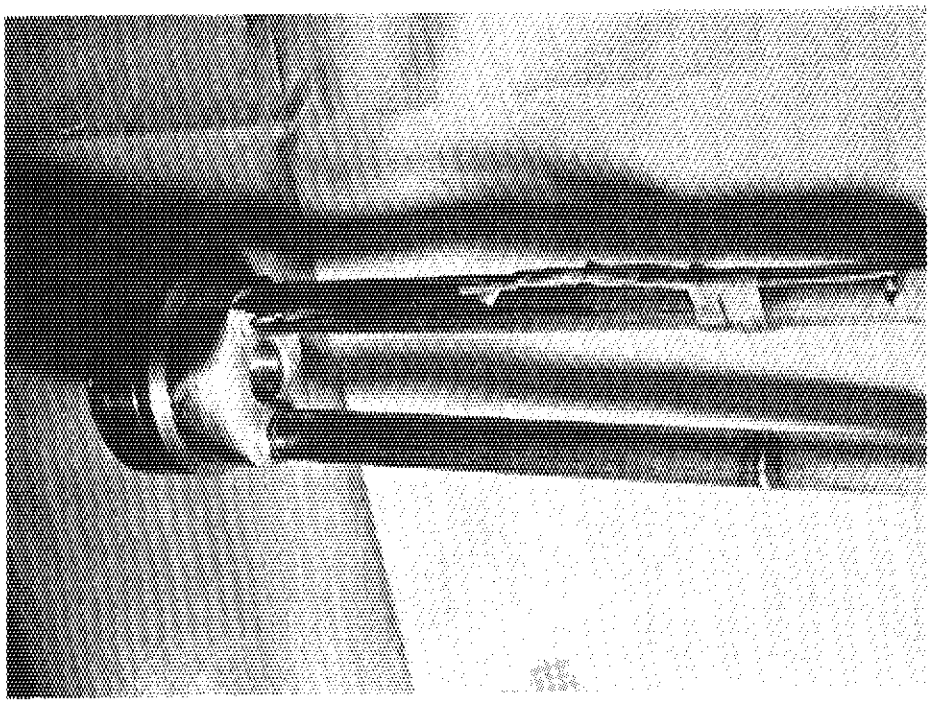

Photo. A-1 Tantalum target used in the experiment